sciendo

Int. J. of Applied Mechanics and Engineering, 2022, vol.27, No.2, pp.1-21
DOI: 10.2478/ijame-2022-0016

INFLUENCE OF SLIP PARAMETER, VISCOUS DISSIPATION AND JOULE HEATING EFFECT ON BOUNDARY LAYER FLOW AND HEAT TRANSFER OVER A POWER-LAW STRETCHING WEDGE-SHAPED SURFACE WITH THE CORRELATION COEFFICIENT AND MULTIPLE REGRESSIONS

MOHAMMAD ALI*
Department of Mathematics, Chittagong University of Engineering and Technology,
Chittagong-4349, BANGLADESH
E-mail: ali.mehidi93@gmail.com

MD. ABDUL ALIM
Department of Mathematics, Bangladesh University of Engineering and Technology,
Dhaka-1000, BANGLADESH

The influence of slip parameter, viscous dissipation, and Joule heating parameter on MHD boundary layer nanofluid flow over a permeable wedge-shaped surface was analysed. The PDEs and the associated boundary conditions were transformed to a set of non-similar ODEs and the obtained system of equations was solved numerically with the help of the spectral quasi-linearization method (SQLM) by applying suitable software. This method helps to identify the accuracy and convergence of the present problem. The current numerical results were compared with previously published work and are found to be similar. The fluid velocity, fluid temperature, and nanoparticle concentration within the boundary layer region for various values of the parameters such as the slip effect, magnetic strength, Prandtl number, Lewis number, stretching ratio, viscous dissipation, suction, Brownian motion, Joule heating, heat generation, and thermophoresis are studied. It is observed that the Brownian motion, Joule heating, viscous dissipation, and thermophoresis lead to decreases in the heat and mass transfer rate. The skin friction coefficient enhances with slip, magnetic, permeability, and suction parameters, but reduces with the Brownian motion, wedge angle, and stretching ratio parameters whereas there is no effect of mixed convection, thermophoresis, heat generation parameters, the Prandtl and Eckert number.

Key words: boundary layer; wedge angle; stretching surface; permeability; slip condition.

1. Introduction

Nanofluids have a wide range of applications in the industrial sector because nanometer-sized particles have unique physical and chemical characteristics. Nanofluids are composite of a solid-liquid dispersion consisting of *1-100 nm*-sized nanoparticles or nanofibers. In recent years, nanofluids have attracted great interest due to the enhancement of their thermal properties. A lot of research work has been done in this field. Water, oil, and ethylene glycol mixtures are known as poor thermal conductivity fluids. These fluids are used as a cooling tool that enhances productivity and reduces operating costs. In recent years, for enhancing the thermal conductivity of these fluids several researchers have studied suspension of nano/microparticles in liquids. But there is no unique fluid model which enhances the thermal conductivity of the fluid. Therefore, over the last few decades, different fluid models have been proposed for enhancing the thermal conductivity of the fluid. Nanofluid is one such fluid. The concept of nanofluid was first introduced by Choi [1] as an advanced type of fluid suspended with the base fluid containing nanometer-sized particles or fibers.

* To whom correspondence should be addressed

Buongiorno [2] found that various factors are responsible for enhancing the thermal conductivity of the nanofluid such as nanoparticle size, inertia, Magnus effect, volume fraction of the nanoparticle, particle agglomeration, Brownian motion, and thermophoresis. Brownian motion and thermophoresis significantly enhance the thermal conductivity of the nanofluid. The two-dimensional laminar *BL* nanofluid flow over a stretching surface is important for various fields such as fiber production, polymer processing, and glass production. Falkner and Skan [3] first introduced the concept of the wedge-shaped surface for discussing the *BL* flow. Nagendramma *et al.* [4] discussed the stretching wedge flow with heat transfer in the presence of a magnetic field and viscous dissipation. It is noticed that the unsteady and wedge-angle parameters are responsible for the flow separation. Ashwini *et al.* [5] analyzed the effect of heat generation and thermal radiation on an unsteady MHD *BL* flow over a wedge. Ramesh *et al.* [6] discussed the MHD *BL* flow over a permeable surface. It is observed that the pressure gradient parameter reduces the thickness of *BL*. Ibrahim [7] investigated the effect of the Brownian motion and thermophoresis on an MHD *BL* nanofluid flow due to porous wedge surfaces. It is noticed that the momentum *BL* thickness reduces for the increasing values of magnetic, permeability, and pressure gradient parameters, but for higher values of *Ec*, Brownian motion (*Nb*), and thermophoresis *Nt* parameters enhance the thickness of thermal *BL*. Nageeb *et al.* [8] analyzed the *BL* mixed convection nanofluid flow over a moving surface with a magnetic effect. Kashmani *et al.* [9] investigated the Soret and Dufour effects on the *BL* flow of a nanofluid over a moving wedge and observed that the temperature gradient enhances for increasing Soret effect but decreases for increasing Dufour number. Waini *et al.* [10] discussed the effect of the stretching ratio on hybrid nanofluid permeable wedge flow and saw that the heat transfer rate is higher in the case of the hybrid nanofluid than the regular nanofluid. Rajab Al-Sayagh [11] studied the free convection heat transfer flow over a *U*-shaped obstacle by taking Al_2O_3 -water nanofluid. Khan and Pop [12] examined the *BL* flow past a wedge moving in a nanofluid. Menni *et al.* [13] presented the hydrodynamic and thermal analysis of water, ethylene glycol, and water-ethylene glycol as base fluids dispersed by aluminum oxide nano-sized solid particles. In addition, Krishna and his collaborators [14 -24] studied a nanofluid flow and heat transfers over an infinite vertical plate with Hall and ion slip effect. Hence, the present problem has been focused on the MHD *BL* nanofluid flow over a wedge-shaped geometry by applying the Buongiorno model. In this work, the system of governing PDEs of momentum and energy has been reduced to non-linear ODEs with boundary conditions by taking appropriate similarity transformations. A spectral quasi-linearization method (SQLM) based on a quasi-linearization method has been applied which was reported by Motsa *et al.* [25]. Based on the aforementioned aspect and applications, the present study has motivated us to scrutinize the effects of physical parameters on the flow field, temperature, and concentration field. Finding the numerical solution encouraged the authors to consider the SQLM. Due to the *BL* region, the effective shape of the solid objects may change leading to changes in pressure distribution, as a result, the overall lift and drag forces change. So, the present problem will help to identify the physical parameters which are responsible for heat and mass transfer characteristics. Therefore, the fluid flow parameters such as the velocity, temperature, and concentration within the *BL* region and the numerical values of the velocity gradient, temperature, and concentration gradient have been discussed graphically and in tabular form. Also, the authors have established a correlation among the controlling parameters and the flow characteristics and developed a multiple regression model.

2. Mathematical model

Let us consider a two-dimensional flow over a stretching wedge-shaped geometry. The *x*-axis is considered parallel to the stretching wedge and the *y*-axis perpendicular to it. It is also assumed that the velocity of the wedge is u_w, U is the free stream velocity, T_w is the wall temperature T_∞ is the free stream temperature, *u* and *v* are the velocity components, respectively. A uniform magnetic field B_0 is applied perpendicularly to the direction of the fluid flow as shown in Fig.1. From this figure, $\Omega = \beta\pi$ is the total wedge angle and β is the wedge angle parameter which is related to the pressure gradient parameter.

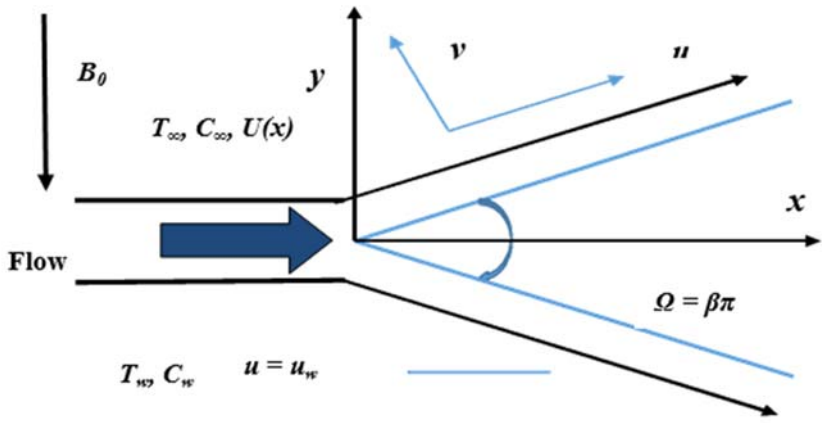

Fig.1. Physical model and coordinate system.

The governing equations of the *BL* nanofluid flow for the present problem are written as follows [2]: continuity equation:

$$\frac{\partial u}{\partial x}+\frac{\partial v}{\partial y}=0\,. \tag{2.1}$$

momentum equation:

$$u\frac{\partial u}{\partial x}+v\frac{\partial u}{\partial y}=U\frac{dU}{dx}+\nu\frac{\partial^2 u}{\partial y^2}+\left(\frac{\sigma B_0^2}{\rho}+\frac{\nu}{K}\right)(U-u)+g\beta^*(T-T_\infty)\,, \tag{2.2}$$

energy equation:

$$\begin{aligned} u\frac{\partial T}{\partial x}+v\frac{\partial T}{\partial y}&=\alpha\frac{\partial^2 T}{\partial y^2}+\tau\left\{D_B\left(\frac{\partial T}{\partial y}\frac{\partial C}{\partial y}\right)+\frac{D_T}{T_\infty}\left(\frac{\partial T}{\partial y}\right)^2\right\}+\\ &+\frac{Q}{\rho c_p}(T-T_\infty)+\frac{\nu}{C_p}\left(\frac{\partial u}{\partial y}\right)^2+\frac{\sigma {B_0}^2 u^2}{\rho C_p}, \end{aligned} \tag{2.3}$$

concentration equation:

$$u\frac{\partial C}{\partial x}+v\frac{\partial C}{\partial y}=D_B\frac{\partial^2 C}{\partial y^2}+\frac{D_T}{T_\infty}\frac{\partial^2 T}{\partial y^2}\,. \tag{2.4}$$

The boundary conditions are:

$$u=u_w=ax^m+N_1\nu\frac{\partial u}{\partial y},\qquad v=v_w,\qquad T=T_w=T_\infty,\quad C=C_w=C_\infty,\qquad \text{at}\quad y=0,$$

$$u=U=bx^m,\quad T=T_\infty,\quad C=C_\infty,\quad \text{at}\quad y=\infty.$$

Here m is the non-linearity factor and is related to the wedge angle parameter β, $N_1 = N\left(ax^m\right)^{-1}$ is the velocity slip factor which changes with the distance x, N is the initial slip factor. The no-slip condition is observed for $N = 0$. For converting the governing Eqs (2.2)-(2.4) into ordinary differential equations, the following transformations have been considered:

$$\eta = y\sqrt{\frac{(1+m)u_w}{2x\nu}}, \quad \psi = \sqrt{\frac{2x\nu u}{(1+m)}}F(\eta), \quad \theta(\eta) = \frac{T-T_\infty}{T_w-T_\infty},$$
$$\varphi(\eta) = \frac{C-C_\infty}{C_w-C_\infty}, \quad u = \frac{\partial\psi}{\partial y}, \quad v = -\frac{\partial\psi}{\partial x}.$$

The converted ordinary differential equations of momentum, temperature ,and concentration are:

$$F'''(\eta) + F(\eta)F''(\eta) + \beta\left(\varepsilon^2 - F'^2(\eta)\right) + \\ + \left(\frac{M+K^*}{1+m}\right)\left(\varepsilon - F'(\eta)\right) + \lambda\theta(\eta) = 0, \tag{2.5}$$

$$\theta''(\eta) + \Pr\left[F(\eta)\theta'(\eta) + Nb\theta'(\eta)\varphi'(\eta) + \right. \\ \left. + Nt\theta'^2(\eta) + Q^*\theta(\eta) + EcF''^2(\eta) + JF'^2(\eta)\right] = 0, \tag{2.6}$$

$$\varphi''(\eta) + \frac{Nt}{Nb}\theta''(\eta) + Le\Pr F(\eta)\varphi'(\eta) = 0. \tag{2.7}$$

The modified boundary conditions:

$$F(\eta) = S, \quad F'(\eta) = 1 + Af''(0), \quad \theta(\eta) = 1, \quad \varphi(\eta) = 1 \quad \text{at} \quad \eta = 0,$$

$$F'(\eta) \to \varepsilon, \quad \theta(\eta) = \varphi(\eta) \to 0, \quad \text{at} \quad \eta \to \infty.$$

The prime denotes derivative with respect to η.

The dimensionless parameters such as the magnetic parameter, stretching ratio parameter, Prandtl number, Brownian motion parameter, pressure gradient, Eckert number, Lewis number, permeability parameter, mixed convection parameter, thermophoresis parameter, Reynold's number, Joule heating parameter, Grashof number, heat generation parameter, suction parameter, and slip parameter respectively are written as:

$$M = \frac{\sigma B_0^2 u_w}{\rho}, \quad \varepsilon = \frac{b}{a}, \quad \Pr = \frac{\nu}{\alpha}, \quad Nb = \frac{\tau D_B\left(C_w - C_\infty\right)}{\nu}, \quad \beta = \frac{2m}{1+m}, \quad Ec = \frac{{u_w}^2}{C_p\left(T_w - T_\infty\right)},$$

$$Le = \frac{\nu}{D_B}, \quad K^* = \frac{\nu x}{KU}, \quad \lambda = \frac{Gr}{\mathrm{Re}^2}, \quad Nt = \frac{\tau D_T\left(T_w - T_\infty\right)}{T_\infty \nu}, \quad \mathrm{Re}_x = \frac{u_w L}{\nu}, \quad J = \frac{\sigma B_0^2 {u_w}^2 L}{\rho a C_p\left(T_w - T_\infty\right)},$$

$$Gr = \frac{g\beta\left(T_w - T_\infty\right)L^3}{\nu^2}, \quad Q^* = \frac{QL\left(T_w - T_\infty\right)}{\rho a c_p}, \quad S = -\sqrt{\frac{(1+m)\nu u}{x}}f(0), \quad A = N_1\sqrt{\frac{a\nu(1+m)}{2}}.$$

The shear stress, heat flux, and mass flux are defined as:

$$\tau_w = -\mu\left(\frac{\partial u}{\partial y}\right)_{y=0}, \qquad q_w = -k\left(\frac{\partial T}{\partial y}\right)_{y=0} \quad \text{and} \quad J_w = -D_B\left(\frac{\partial C}{\partial y}\right)_{y=0}.$$

Therefore, the skin friction coefficient C_f, the local Nusselt Nu_x, and local Sherwood numbers Sh_x can be written as:

$$C_f = -\sqrt{\frac{2(1+m)}{\mathrm{Re}_x}}F''(0), \quad Nu_x = -\sqrt{\frac{(1+m)\mathrm{Re}_x}{2}}\theta'(0), \quad Sh_x = -\sqrt{\frac{(1+m)\mathrm{Re}_x}{2}}\varphi'(0).$$

3. Methodology

Bellman and Kalaba [26] were the first to solve nonlinear ODEs and PDEs by applying the quasi-linearization method (QLM) about half a century ago. Thus, for numerical solutions, we need to choose an appropriate numerical technique. The spectral quasi-linearization method (SQLM) [25] is a combination of two methods such as the QLM and the Chebyshev spectral collocation method (CSCM). The QLM is used to linearize the non-linear ODEs into linear ODEs. The QLM assumes that the difference between the approximate solution at the present iteration and the previous iteration is very small. The quadratic convergence property is the advantage of this technique. Three to six iterations are needed for getting five-digit accuracy if the technique converges. The numerical simulation of the present problem is obtained with the help of SQLM [25] which gives highly accurate results. The similarity variable is taken as $\eta \to \infty$ but the present simulation has been performed for a finite domain of $\eta = 5$, 5, and 10 for velocity, temperature, and concentration profiles respectively. Therefore, the dimensionless velocity, temperature, and concentration distribution within the *BL* asymptotically tend to a free stream velocity to satisfy the far-field boundary conditions. All other parameters are considered to be some fixed values for finding the self-similar solution. So, applying SQLM, the system of Eqs (2.5)-(2.7) has been transformed into the following iterative sequence of linear differential equations

$$a_{0,r}\frac{\partial^3 F_{r+1}}{\partial\eta^3} + a_{1,r}\frac{\partial^2 F_{r+1}}{\partial\eta^2} + a_{2,r}\frac{\partial F_{r+1}}{\partial\eta} + a_{3,r}F_{r+1} + a_{4,r}\theta_{r+1} = R_{1,r}, \tag{3.1}$$

$$\begin{aligned} &b_{0,r}\frac{\partial^2\theta_{r+1}}{\partial\eta^2} + b_{1,r}\frac{\partial\theta_{r+1}}{\partial\eta} + b_{2,r}\theta_{r+1} + b_{3,r}\frac{\partial^2 F_{r+1}}{\partial\eta^2} + \\ &+b_{4,r}\frac{\partial F_{r+1}}{\partial\eta} + b_{5,r}F_{r+1} + b_{6,r}\frac{\partial\varphi_{r+1}}{\partial\eta} = R_{2,r}, \end{aligned} \tag{3.2}$$

$$e_{0,r}\frac{\partial^2\varphi_{r+1}}{\partial\eta^2} + e_{1,r}\frac{\partial\varphi_{r+1}}{\partial\eta} + e_{2,r}\frac{\partial F_{r+1}}{\partial\eta} + e_{3,r}\frac{\partial^2\theta_{r+1}}{\partial\eta^2} = R_{3,r} \tag{3.3}$$

where the variable coefficients obtained from the previous iteration are given by:

$$a_{0,r} = 1, \;\; a_{1,r} = F_r, \;\; a_{2,r} = -2\beta F_r' - \left(\frac{M+K^*}{1+m}\right), \;\; a_{3,r} = F_r'', \;\; a_{4,r} = \lambda, \;\; b_{0,r} = 1, \;\; b_{2,r} = \mathrm{Pr}Q^*,$$

$$b_{1,r} = \Pr\left(F_r + Nb\varphi'_r + 2Nt\theta'_r\right), \quad b_{3,r} = 2EcF'', \quad b_{4,r} = 2JF'_r, \quad b_{5,r} = \Pr\theta'_r, \quad b_{6,r} = \Pr Nb\theta'_r,$$

$$e_{0,r} = 1, \quad e_{1,r} = Le\Pr F_r, \quad e_{2,r} = -Le\Pr\beta F'_r, \quad e_{3,r} = \frac{Nt}{Nb}, \quad e_{4,r} = -Le\Pr\beta\varphi_r, \quad e_{5,r} = Le\Pr\varphi'_r.$$

The terms $R_{1,r}(\eta), R_{2,r}(\eta),$ and $R_{3,r}(\eta)$ are defined as:

$$R_{1,r}(\eta) = a_{0,r}F'''_r + a_{1,r}F''_r + a_{2,r}F'_r + a_{3,r}F_r + a_{4,r}\theta_r - F\left[\eta, F_r, F'_r, F''_r \ldots\ldots F^n_r\right] =$$
$$= F_r F''_r - \beta F'^2_r - \beta\varepsilon^2 - \varepsilon\left(\frac{M + K^*}{1+m}\right),$$

$$R_{2,r}(\eta) = b_{0,r}\theta''_r + b_{1,r}\theta'_r + b_{2,r}\theta_r + b_{3,r}F''_r + b_{4,r}F'_r + b_{5,r}F_r - F\left[\eta, F_r, F'_r, F''_r \ldots\ldots F^n{}_r\right] =$$
$$= \Pr\left[F_r\theta'_r - \beta F'_r\theta_r + Nb\theta'_r\varphi'_r + Nt\left(\theta'_r\right)^2 + Ec\left(F''_r\right)^2 + J\left(F'_r\right)^2\right],$$

$$R_{3,r}(\eta) = e_{0,r}\varphi''_r + e_{1,r}\varphi'_r + e_{2,r}\varphi_r + e_{3,r}\theta''_r + e_{4,r}F'_r + e_{5,r}F_r - F\left[\eta, F_r, F'_r, F''_r \ldots\ldots F^n{}_r\right] =$$
$$= Le\Pr\left(F_r\varphi'_r - \beta F'_r\varphi_r\right).$$

Evaluating Eqs (3.1)-(3.3) by the collocation points and Chebyshev derivatives we got a vector-matrix form such as:

$$\begin{bmatrix} A_{11} & A_{12} & A_{13} \\ A_{21} & A_{22} & A_{23} \\ A_{31} & A_{32} & A_{33} \end{bmatrix} \begin{bmatrix} F_{r+1} \\ \theta_{r+1} \\ \varphi_{r+1} \end{bmatrix} = \begin{bmatrix} R_{1,r} \\ R_{2,r} \\ R_{3.r} \end{bmatrix}$$

where

$$A_{11} = a_{0,r}D^3 + a_{1,r}D^2 + a_{2,r}D + a_{3,r}, \quad A_{12} = a_{4,r}, \quad A_{13} = I,$$

$$A_{21} = b_{3,r}D + b_{4,r}, \quad A_{22} = b_{0,r}D^2 + b_{1,r}D + b_{2,r}, \quad A_{23} = b_{5,r}D,$$

$$A_{31} = e_{4,r}D + e_{5,r}, \quad A_{32} = e_{3,r}D^2, \quad A_{33} = e_{0,r}D^2 + e_{1,r}D + e_{2,r},$$

and

$$D = \left(\frac{2}{l_\infty}\right)\mathbb{k}, \qquad \mathbb{k} \text{ is a } (N+1)\times(N+1) \text{ Chebyshev differentiation matrix.}$$

The modified boundary conditions are:

$$F_{r+1}(\eta_0) = F_w, \quad F'_{r+1}(\eta_0) = 1, \quad \theta_{r+1}(\eta_0) = 1, \quad \varphi_{r+1}(\eta_0) = 1, \quad R_r(\eta_N) = 1 \quad \text{at} \quad \eta = 0,$$

$$F_{r+1}(\eta_N) = F_w, \quad F'_{r+1}(\eta_N) \to \varepsilon, \quad \theta_{r+1}(\eta_N) = \varphi_{r+1}(\eta_0) \to 0, \quad R_r(\eta_{N+1}) \to \varepsilon \quad \text{as} \quad \eta \to \infty.$$

4. Results and discussion

The non-linear ODEs of the present problem are solved by applying SQLM. The convergence criteria of the solution are performed by the use of solution-based errors. These errors are defined by the differences between approximate solutions at the previous and present iteration levels t and $t+1$, respectively. The error norms are defined as:

$$Error_f = \max_{0\le i\le N}\left\|F_{t+1,i}-F_{t,i}\right\|,\quad Error_\theta = \max_{0\le i\le N}\left\|\theta_{t+1,i}-\theta_{t,i}\right\| \quad \text{and} \quad Error_\varphi = \max_{0\le i\le N}\left\|\varphi_{t+1,i}-\varphi_{t,i}\right\|.$$

The infinity norms of the residual errors are defined as:

$$\left\|\mathrm{Re}s(F)\right\|_\infty = \left\|F''' + FF'' + \beta\left(1-F'^2\right) + \left(\frac{M+K^*}{1+m}\right)(1-F') + \lambda\theta\right\|,$$

$$\left\|\mathrm{Re}s(\theta)\right\|_\infty = \left\|\theta'' + \mathrm{Pr}\left[F\theta' + Nb\theta'\varphi' + Nt\theta'^2 + Q^*\theta + EcF''^2 + JF'^2\right]\right\|,$$

$$\left\|\mathrm{Re}s(\varphi)\right\|_\infty = \left\|\varphi'' + \frac{Nt}{Nb}\theta'' + Le\,\mathrm{Pr}\,F\varphi'\right\|.$$

The impact of physical parameters on velocity $f'(\eta)$, temperature $\theta(\eta)$, and concentration $\varphi(\eta)$ profile is shown graphically. The numerical values of the skin friction $\left(C_f\sqrt{\mathrm{Re}_x}\right)$, Nusselt number $\left(Nu_x\left(\sqrt{\mathrm{Re}_x}\right)^{-1}\right)$, and Sherwood number $\left(Sh_x\left(\sqrt{\mathrm{Re}_x}\right)^{-1}\right)$ which are equivalent to the rate of velocity $f''(0)$, rate of heat transfer $\theta'(0)$, and rate of concentration are shown in Tabs 1 and 2, respectively. The computations were done by taking $N=60$ collocation points and solution-based errors are defined for the convergence of the numerical method.

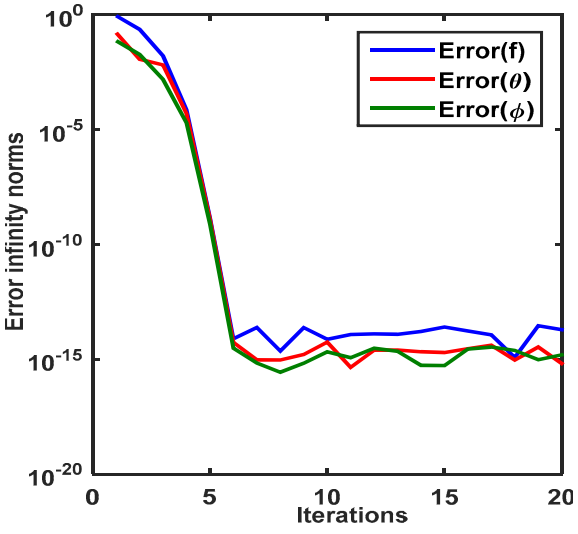

Fig.1a. Error infinity norms.

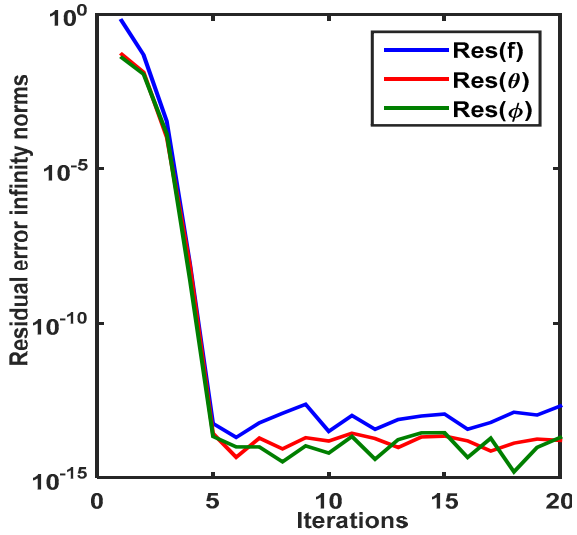

Fig.1b. Residual error infinity norms for $f(\eta)$, $\theta(\eta)$ and $\varphi(\eta)$.

So, Figs 1a and 1b show the convergence and accuracy of the present problem. Figure 1a represents the infinity norms with iterations. The error infinity norm decreases with the increasing number of iterations that confirms the convergence of the present method. So the present method converges after six iterations. Figure 1b represents the residual error norms of less than 10^{-14} for $f(\eta)$, $\theta(\eta)$ and $\varphi(\eta)$ after five iterations. It is seen that the residual error decreases with increasing the iterations. This proves the validity of the present method. The errors show that the SQLM is accurate giving errors of less than 10^{-15} within the sixth iteration. Figures 1a and 1b show the convergence and accuracy of the present method. It is observed that the error infinity norm reduces with an increase in the number of iterations and after six iterations the method converges. Also, the residual error infinity norms reduce against the number of iterations which ensures the accuracy of the method. The SQLM achieves an accuracy of order 10^{-15} after the fifth iteration showing that the method is highly accurate. The solution has been obtained by taking $M = 5.0$, $Nb = 0.1$, $Nt = 0.1$, $K^* = 0.2$, $\beta = 36^\circ$, $\Pr = 1.0$, $S = 10.0$, $Le = 10.0$, $Ec = 0.2$, $Q^* = 0.2$, $J = 0.1$ and $\lambda = 0.2$. The results have been shown graphically and also in the tabular form in the following sub-sections.

4.1. Velocity profile

Figures 2a-2g demonstrate the effect of the magnetic parameter M, pressure gradient parameter m, stretching ratio parameter ε, permeability parameter K^*, suction (S) parameter, slip parameter A, and wedge angle parameter β, on the fluid velocity within the BL region. The velocity profiles show that inside the BL region the transport rate decreases with the increasing distance η of the surface. In all cases, the fluid velocity within the BL region vanishes at a certain distance from the surface $(\text{at } \eta = 5)$.

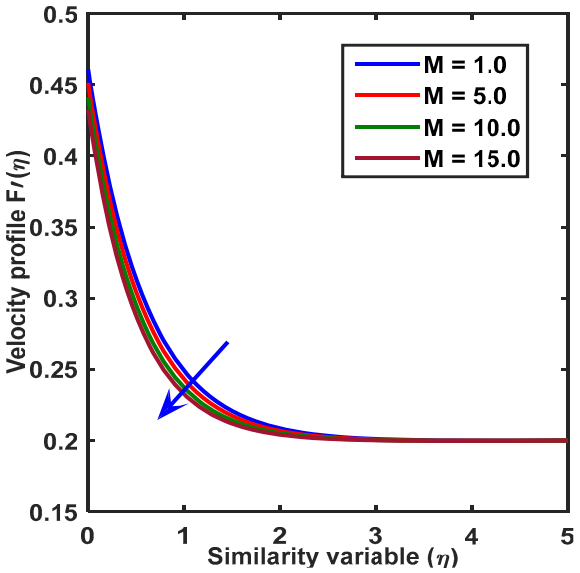

Fig.2a. Velocity profile with η for the variation of M.

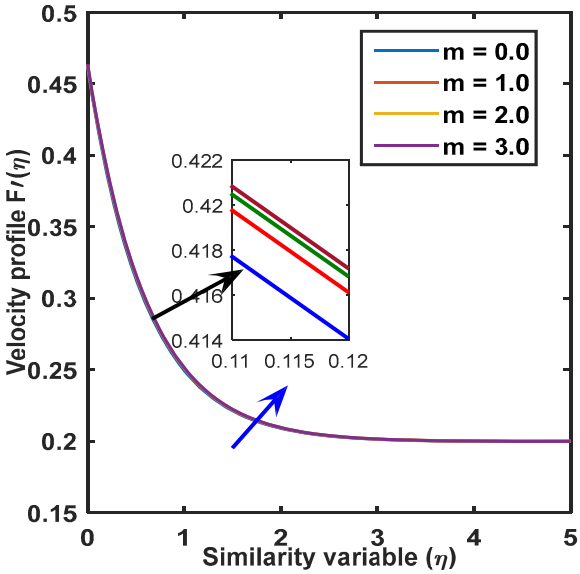

Fig.2b. Velocity profile with η for the variation Nb.

This figure demonstrates that within the BL region the fluid velocity enhances for rising values of m and ε but a reverse trend has been observed for the magnetic parameter, permeability parameter, wedge angle parameter, suction parameter, and slip parameter, respectively. From Eq.(2.2), the parameter M can be explained by the

term $\frac{\sigma B_0^{\,2}}{\rho}(U-u)$. This term is the combination of two forces such as the pressure force $\left(\frac{\sigma B_0^{\,2}}{\rho}U\right)$ and Lorentz force $\left(\frac{\sigma B_0^{\,2}}{\rho}u\right)$. When the Lorentz force dominates the pressure force $(u>U_\infty)$, then the fluid velocity decreases within the *BL* region.

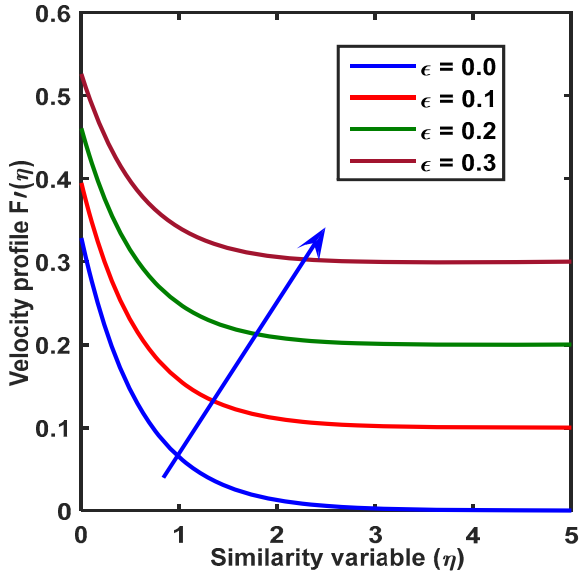

Fig.2c. Velocity profile with η for the variation ε.

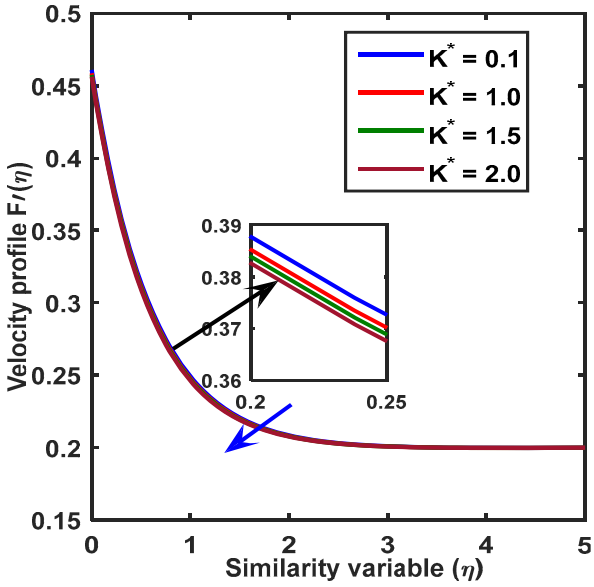

Fig.2d. Velocity profile with η for the variation K^*

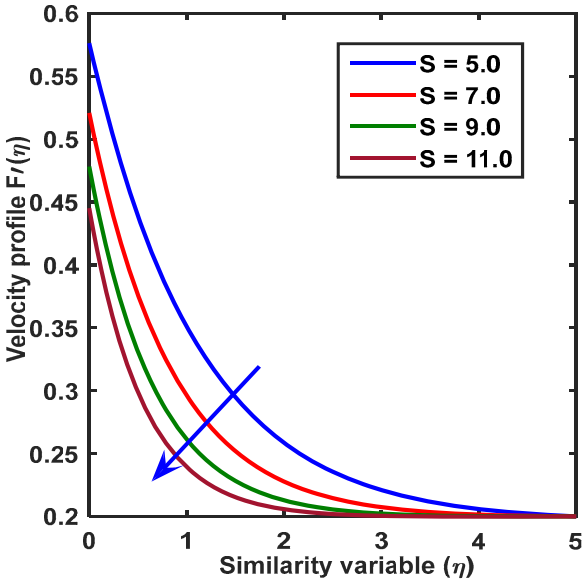

Fig.2e. Velocity profile with η for the variation *S*.

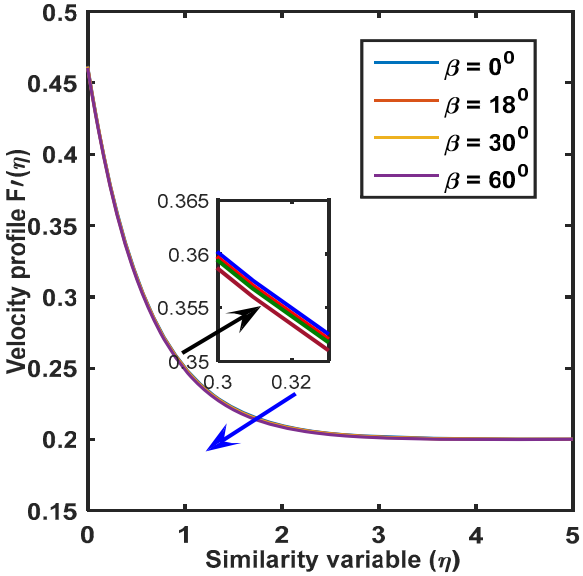

Fig.2f. Velocity profile with η for the variation β.

The physical behavior of the parameter ε is that when the surface velocity dominates on the free stream velocity then fluid velocity is enhanced. The higher values of the parameter K^* cause higher resistance against the fluid motion and as a result the velocity of fluid decreases. The physics of the parameter β is that the uplifting values of this parameter mean to increase the shape and size of the wedge-shaped geometry and as a result the fluid velocity decreases. Due to slip conditions, the velocity of flow near the surface is not the same as the stretching surface velocity. With the increase in A the slip velocity increases and therefore fluid velocity reduces within the *BL* region because due to the slip condition, the pulling of the stretching surface can be only partly transmitted to the fluid. It is seen that A has a substantial effect on the fluid flow properties. Therefore, from these figures, it is noticed that the *BL* thickness enhances for uplifting values of M, K^*, β, A and S because the velocity of fluid decreases within the *BL* region but a reverse result arises for the parameters m and ε respectively.

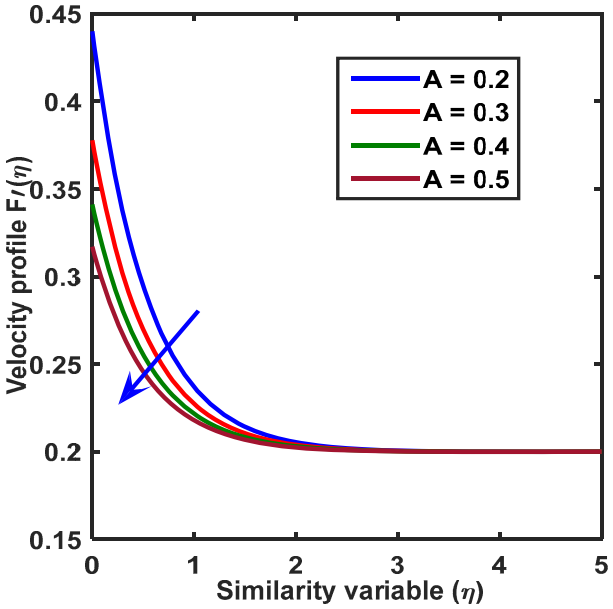

Fig.2g. Velocity profile with η for the variation A.

4.2. Temperature profile

Figures 3a-3g present the temperature distribution for different values of the thermophoresis parameter *Nt*, Brownian motion *Nb*, Joule heating parameter *J*, suction parameter *S*, heat generation parameter Q^*, slip parameter *A*, and viscous dissipation parameter *Ec*. From these figures, it is observed that the temperature within the *BL* region decreases by enhancing the values of *S*. The temperature within the *BL* region enhances for uplifting values of the Brownian motion and thermophoresis parameters because the nanoparticles within the fluid are moved randomly, as a result, the collision between nanoparticles and fluid molecules accelerates. For this reason, the kinetic energy is transformed into thermal energy and as a result the temperature within the *BL* region is enhanced. A similar result arises for the Joule heating, Eckert number, and heat source parameters because extra heat is produced as a result of the fluid particles moving from a hotter region to a cooler region which causes quicker heat transfer from the hotter surface to the surrounding fluid. Thus, it is seen that the thermal *BL* thickness enhances for the parameters *Nb*, *Nt*, *J*, Q^*, *A* and *Ec* respectively because the temperature gradient decreases but a reverse results are observed for the variation of the suction parameter.

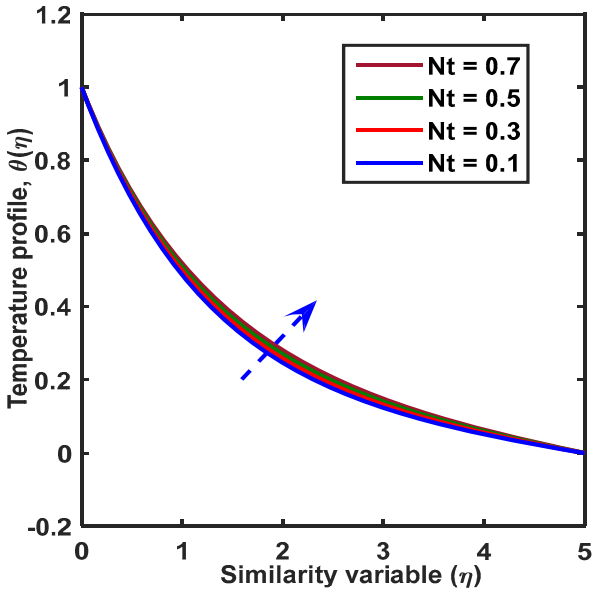

Fig.3a. Temperature profile with η for the variation of *Nt*.

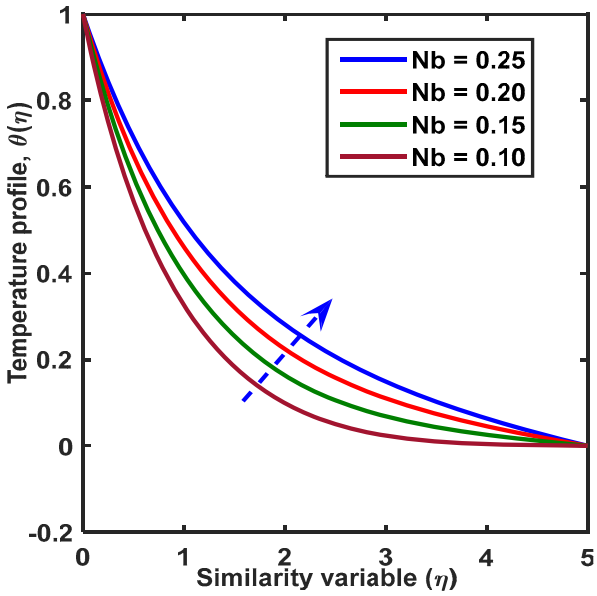

Fig.3b. Temperature profile with η for the variation of *Nb*.

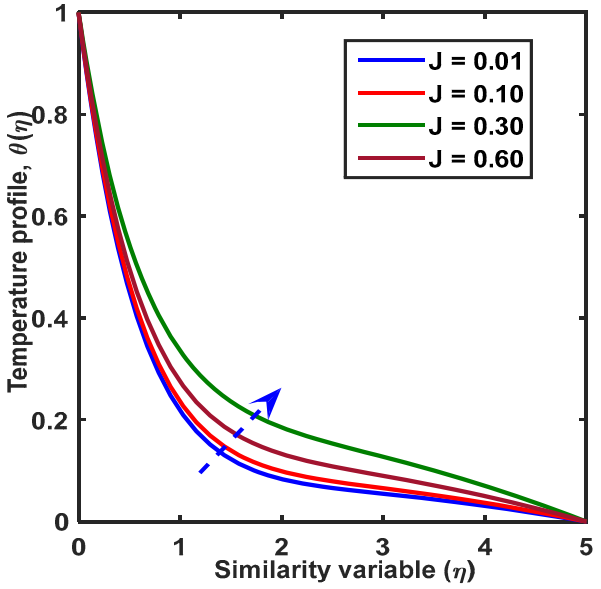

Fig.3c. Temperature profile with η for the variation of *J*.

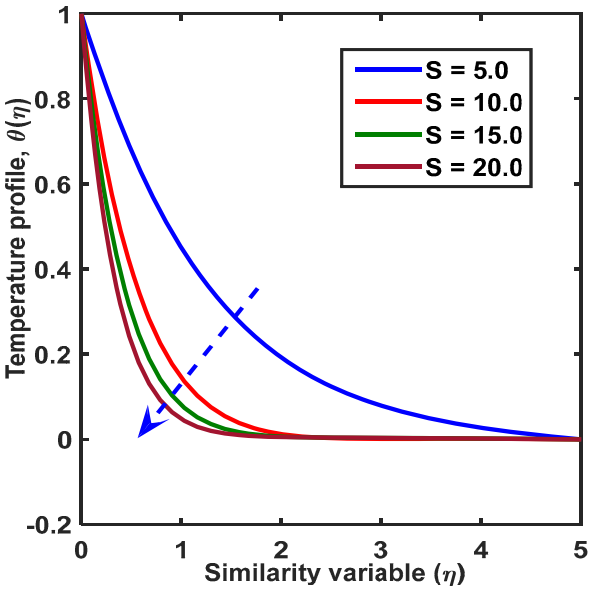

Fig.3d. Temperature profile with η for the variation of *S*.

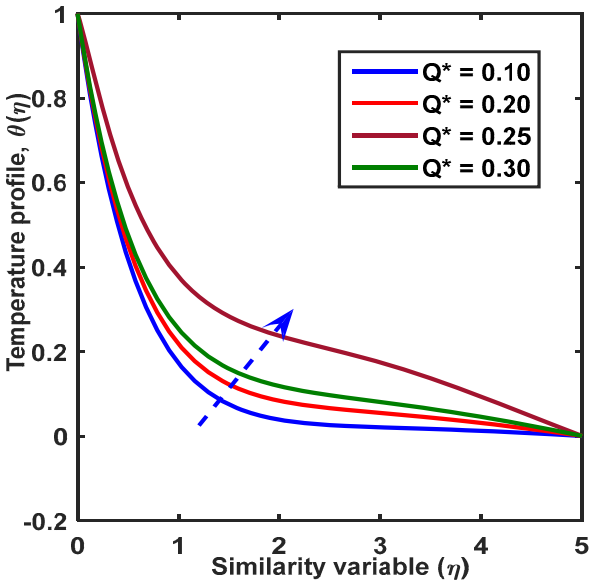

Fig.3e. Temperature profile with η for the variation of Q^*.

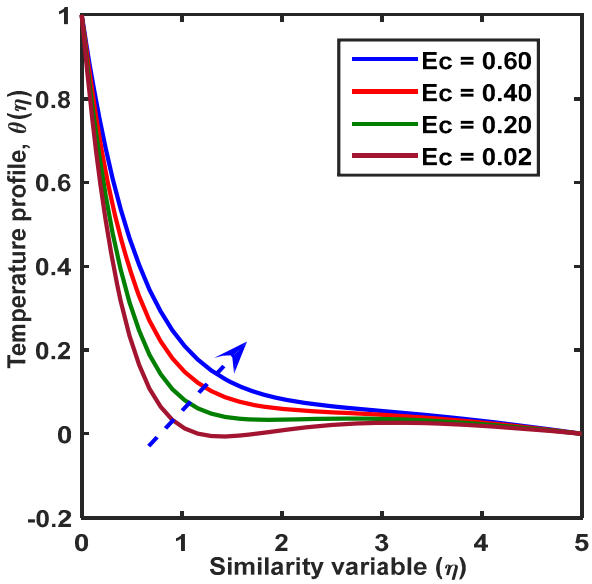

Fig.3f. Temperature profile with η for the variation of *Ec*.

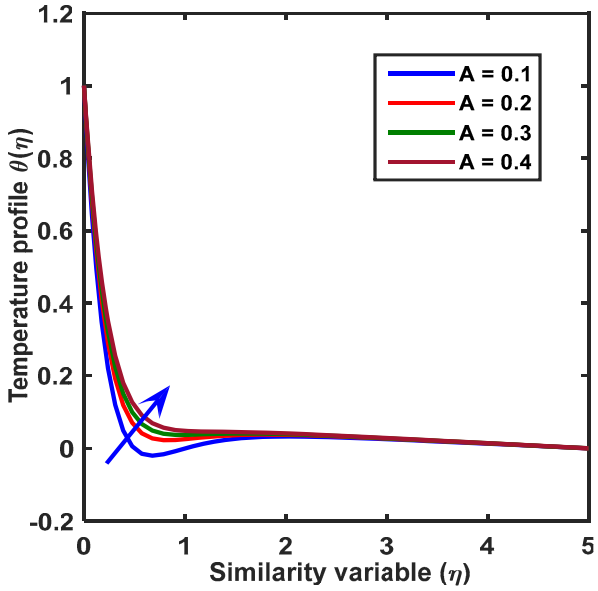

Fig.3g. Temperature profile with η for the variation of *A*.

4.3. Concentration profile

The variations of the Prandtl number Pr, Lewis number *Le*, Brownian motion *Nb*, thermophoresis parameter *Nt*, heat source parameter Q^* and suction parameter *S* on concentration profile are depicted in Figs 4a-4f. The concentration reduces within the *BL* region for uplifting values of Pr, *Le*, *Nb*, Q^* and *S*, respectively, but increases for rising values of *Nt*. This happens due to the random motion of the nanoparticles and as a result concentration decreases. The concentration enhances within the *BL* region because the thermophoresis

accelerates the fluid particles. As a result particles move quickly from the hotter area to the surrounding cold area. The uplifting values of the Lewis number mean reducing the mass diffusivity which causes a decrease in concentration. From concentration profiles, it is noticed that the *BL* thickness of concentration reduces for an increment of Pr, *Le*, *Nb*, Q^* and *S* but a reverse trend arises for the parameter *Nt*.

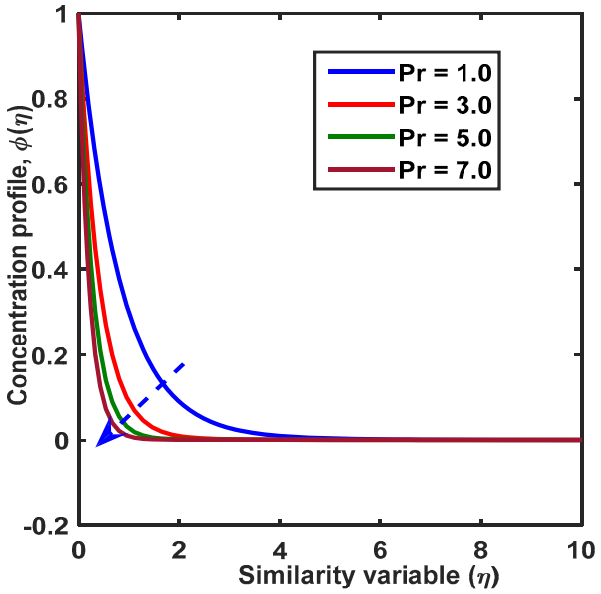

Fig.4a. Concentration profile with η for the variation of Pr.

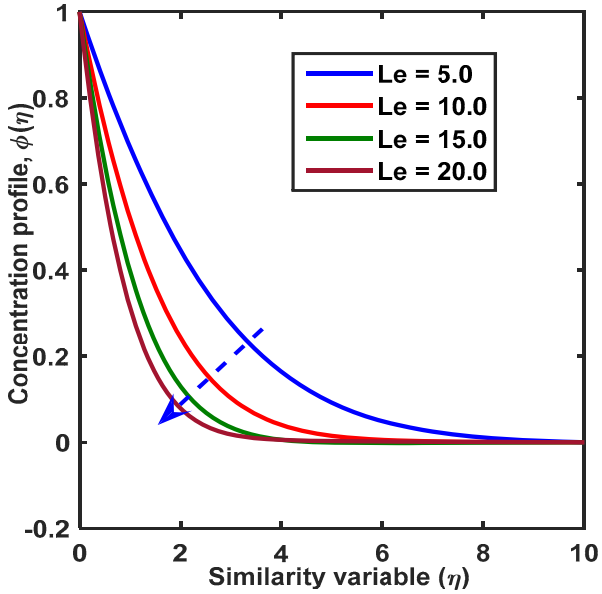

Fig.4b. Concentration profile with η for the variation of *Le*.

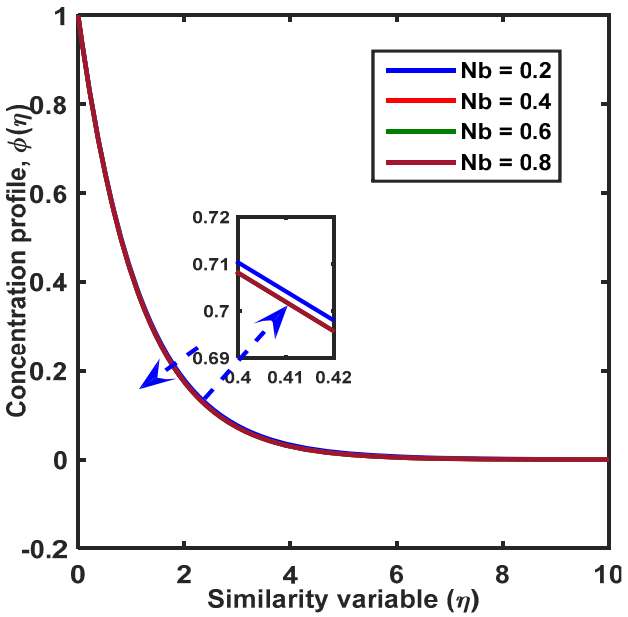

Fig.4c. Concentration profile with η for the variation of *Nb*.

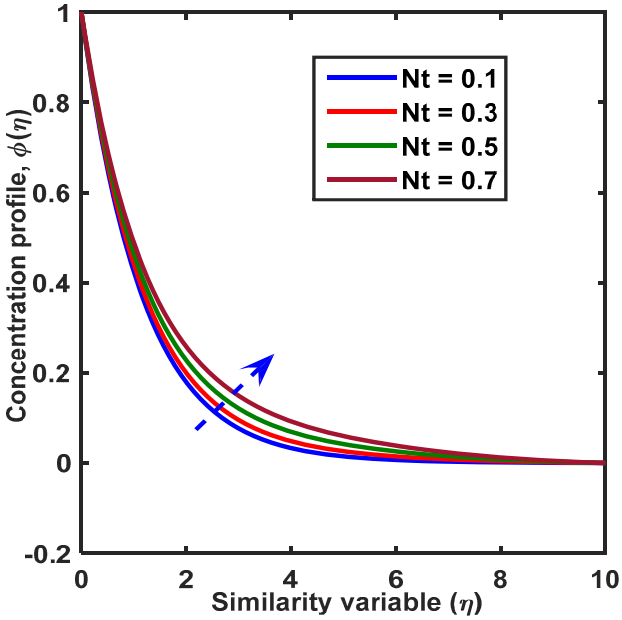

Fig.4d. Concentration profile with η for the variation of *Nt*.

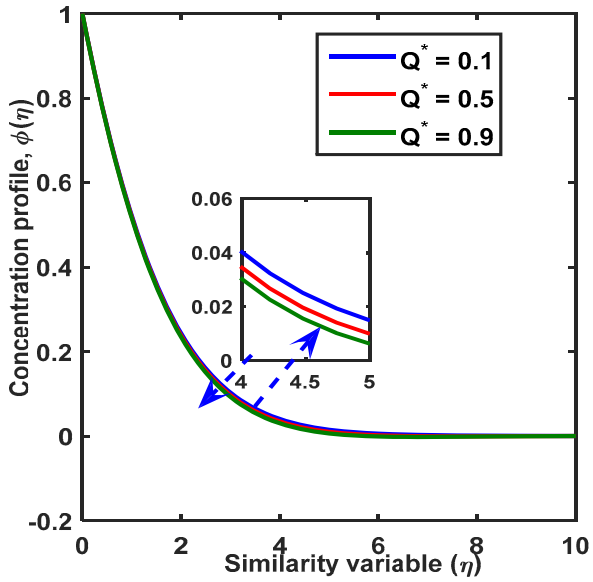

Fig.4e. Concentration profile with η for the variation of Q^*.

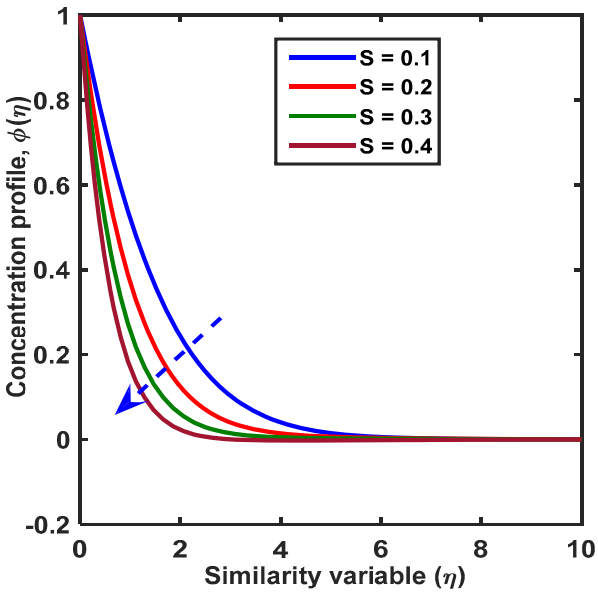

Fig.4f. Concentration profile with η for the variation of *S*.

4.4. Velocity, temperature and concentration gradient

The numerical values of velocity, temperature, and concentration gradients are displayed in Tab.1 for the dimensionless parameters. From this table, it is noticed that the velocity gradient reduces for ε but enhances for K^*, *M*, β, and *S* whereas there is no effect for λ, *Nb*, *Nt*, *J* and *Ec*. There is no effect of the parameter K^* on the temperature gradient but the parameters ε, K^*, *M*, λ, *Nt*, *A* and *J* decrease the temperature gradient, whereas β, *S*, and *Ec* increase the temperature gradient. The mass transfer rate enhances for enhancing the values of *Nb* and S but reduces for *Nt*. On the other hand, ε, β, λ, K^* and *M* do not affect the mass transfer rate.

Table 1. Computed values of velocity, temperature, and concentration gradient for different values of the mentioned parameters.

ε	K^*	*M*	β	λ	*S*	*Nb*	*Nt*	*A*	*J*	*Ec*	$f''(0)$	$\lvert-\theta'(0)\rvert$	$\lvert-\varphi'(0)\rvert$
0.0	*0.2*	*10.0*	*0.2*	*0.2*	*10.0*	*0.2*	*0.2*	*0.2*	*0.1*	*0.2*	*3.4952*	*1.3081*	*-3.7598*
0.1	*0.2*	*10.0*	*0.2*	*0.2*	*10.0*	*0.2*	*0.2*	*0.2*	*0.1*	*0.2*	*3.1469*	*1.0126*	*-3.8490*
0.2	*0.2*	*10.0*	*0.2*	*0.2*	*10.0*	*0.2*	*0.2*	*0.2*	*0.1*	*0.2*	*2.7993*	*0.7192*	*-3.9368*
0.2	*0.1*	*10.0*	*0.2*	*0.2*	*10.0*	*0.2*	*0.2*	*0.2*	*0.1*	*0.2*	*2.6920*	*0.8047*	*-3.8857*
0.2	*1.0*	*10.0*	*0.2*	*0.2*	*10.0*	*0.2*	*0.2*	*0.2*	*0.1*	*0.2*	*2.7049*	*0.7945*	*-3.8938*
0.2	*1.5*	*10.0*	*0.2*	*0.2*	*10.0*	*0.2*	*0.2*	*0.2*	*0.1*	*0.2*	*2.7118*	*0.7890*	*-3.8978*
0.2	*0.5*	*1.0*	*0.2*	*0.2*	*10.0*	*0.2*	*0.2*	*0.2*	*0.1*	*0.2*	*2.6935*	*0.8035*	*-3.8867*
0.2	*0.5*	*5.0*	*0.2*	*0.2*	*10.0*	*0.2*	*0.2*	*0.2*	*0.1*	*0.2*	*2.7464*	*0.7615*	*-3.9152*
0.2	*0.5*	*10.0*	*0.2*	*0.2*	*10.0*	*0.2*	*0.2*	*0.2*	*0.1*	*0.2*	*2.7993*	*0.7192*	*-3.9368*

Cont. Table 1. Computed values of velocity, temperature, and concentration gradient for different values of the mentioned parameters.

ε	K^*	M	β	λ	S	Nb	Nt	A	J	Ec	$f''(0)$	$\lvert-\theta'(0)\rvert$	$\lvert-\varphi'(0)\rvert$
0.2	*0.5*	*10.0*	*0.0*	*0.2*	*10.0*	*0.2*	*0.2*	*0.2*	*0.1*	*0.2*	*2.8066*	*0.7126*	*-3.9401*
0.2	*0.5*	*10.0*	*0.1*	*0.2*	*10.0*	*0.2*	*0.2*	*0.2*	*0.1*	*0.2*	*2.8031*	*0.7159*	*-3.9385*
0.2	*0.5*	*10.0*	*0.3*	*0.2*	*10.0*	*0.2*	*0.2*	*0.2*	*0.1*	*0.2*	*2.7946*	*0.7237*	*-3.9345*
0.2	*0.5*	*10.0*	*0.2*	*0.2*	*10.0*	*0.2*	*0.2*	*0.2*	*0.1*	*0.2*	*2.8007*	*0.7181*	*-3.9374*
0.2	*0.5*	*10.0*	*0.2*	*0.5*	*10.0*	*0.2*	*0.2*	*0.2*	*0.1*	*0.2*	*2.8007*	*0.7179*	*-3.9375*
0.2	*0.5*	*10.0*	*0.2*	*1.0*	*10.0*	*0.2*	*0.2*	*0.2*	*0.1*	*0.2*	*2.8007*	*0.7176*	*-3.9376*
0.2	*0.5*	*10.0*	*0.2*	*0.2*	*5.0*	*0.2*	*0.2*	*0.2*	*0.1*	*0.2*	*2.4095*	*0.5652*	*1.9574*
0.2	*0.5*	*10.0*	*0.2*	*0.2*	*7.0*	*0.2*	*0.2*	*0.2*	*0.1*	*0.2*	*2.5853*	*0.6559*	*2.7381*
0.2	*0.5*	*10.0*	*0.2*	*0.2*	*10.0*	*0.2*	*0.2*	*0.2*	*0.1*	*0.2*	*2.8007*	*0.7181*	*-3.9374*
0.2	*0.5*	*10.0*	*0.2*	*0.2*	*10.0*	*0.1*	*0.2*	*0.2*	*0.1*	*0.2*	*2.8007*	*0.7181*	*7.8762*
0.2	*0.5*	*10.0*	*0.2*	*0.2*	*10.0*	*0.3*	*0.2*	*0.2*	*0.1*	*0.2*	*2.8007*	*0.7181*	*2.6244*
0.2	*0.5*	*10.0*	*0.2*	*0.2*	*10.0*	*0.5*	*0.2*	*0.2*	*0.1*	*0.2*	*2.8007*	*0.7181*	*1.5740*
0.2	*0.5*	*10.0*	*0.2*	*0.2*	*10.0*	*0.2*	*0.1*	*0.2*	*0.1*	*0.2*	*2.8007*	*0.7204*	*1.9676*
0.2	*0.5*	*10.0*	*0.2*	*0.2*	*10.0*	*0.2*	*0.3*	*0.2*	*0.1*	*0.2*	*2.8007*	*0.7159*	*5.9078*
0.2	*0.5*	*10.0*	*0.2*	*0.2*	*10.0*	*0.2*	*0.5*	*0.2*	*0.1*	*0.2*	*2.8007*	*0.7115*	*9.8507*
0.2	*0.5*	*10.0*	*0.2*	*0.2*	*10.0*	*0.2*	*0.2*	*0.1*	*0.1*	*0.2*	*4.3097*	*1.3215*	*-3.8338*
0.2	*0.5*	*10.0*	*0.2*	*0.2*	*10.0*	*0.2*	*0.2*	*0.2*	*0.1*	*0.2*	*2.8007*	*0.7181*	*-3.9374*
0.2	*0.5*	*10.0*	*0.2*	*0.2*	*10.0*	*0.2*	*0.2*	*0.3*	*0.1*	*0.2*	*2.0745*	*0.4407*	*-3.9870*
0.2	*0.5*	*10.0*	*0.2*	*0.2*	*10.0*	*0.2*	*0.2*	*0.2*	*0.10*	*0.2*	*2.8007*	*0.7181*	*-3.9374*
0.2	*0.5*	*10.0*	*0.2*	*0.2*	*10.0*	*0.2*	*0.2*	*0.2*	*0.15*	*0.2*	*2.8003*	*0.5410*	*-3.9926*
0.2	*0.5*	*10.0*	*0.2*	*0.2*	*10.0*	*0.2*	*0.2*	*0.2*	*0.20*	*0.2*	*2.7999*	*0.3631*	*-4.0470*
0.2	*0.5*	*10.0*	*0.2*	*0.2*	*10.0*	*0.2*	*0.2*	*0.2*	*0.1*	*0.2*	*2.7995*	*0.7192*	*-3.9368*
0.2	*0.5*	*10.0*	*0.2*	*0.2*	*10.0*	*0.2*	*0.2*	*0.2*	*0.1*	*0.4*	*2.8002*	*1.7728*	*-3.7468*
0.2	*0.5*	*10.0*	*0.2*	*0.2*	*10.0*	*0.2*	*0.2*	*0.2*	*0.1*	*0.6*	*2.8010*	*2.8151*	*-3.5633*

5. Comparison

To ensure the validity of the present results they are compared with Mohammadi *et al.* [27] in Tab.2. From this table, it is concluded that the results show a good agreement under particular cases. This comparison ensures the validity of the present problem.

Table 2. Comparison of temperature gradient for different values of Pr when other parameters are zero.

	Mohammadi *et al.*	Present results	Presentence of error
Pr	*-θ'(0)*	*- θ'(0)*	*- θ'(0)*
0.72	*0.501508*	*0.5044*	*-0.6%*
6.0	*1.107140*	*1.0912*	*-0.0014%*
10.0	*1.317881*	*1.3215*	*0.3%*

6. Correlation and regression analysis of local skin friction coefficient

From Tab.3, it is observed that the velocity gradient is positively correlated with the parameters K^*, M, and S, but negatively correlated with ε and A, whereas there is no correlation with β, λ, Nb, Nt, J, and Ec.

Table 3. The correlation coefficient of the velocity, temperature, and concentration gradient for the mentioned parameters.

	ε	K^*	M	β	λ	S	Nb	Nt	A	J	Ec	$f''(0)$	$\theta'(0)$	$\varphi'(0)$
ε	1.0													
K^*	0.3	1.0												
M	-0.1	0.0	1.0											
β	0.0	0.0	0.0	1.0										
λ	0.1	0.0	0.1	0.0	1.0									
S	-0.1	0.0	-0.1	0.0	0.1	1.0								
Nb	0.0	0.0	0.0	0.0	0.0	0.0	1.0							
Nt	0.0	0.0	0.0	0.0	0.0	0.0	0.0	1.0						
A	0.0	0.0	0.0	0.0	0.0	0.0	0.0	0.0	1.0					
J	0.1	0.0	0.1	0.0	-0.1	0.1	0.0	0.0	0.0	1.0				
Ec	0.1	0.0	0.1	0.0	-0.1	0.1	0.0	0.0	0.0	-0.1	1.0			
$f''(0)$	-0.4	0.2	0.1	0.0	0.0	0.3	0.0	0.0	-0.8	0.0	0.0	1.0		
$\theta'(0)$	-0.2	-0.1	0.0	0.0	-0.1	0.1	-0.2	-0.3	-0.3	-0.2	-0.9	0.3	1.0	
$\varphi'(0)$	0.1	0.0	0.1	0.1	-0.1	-0.3	0.1	0.5	0.0	-0.1	-0.1	-0.1	-0.2	1.0

Table 4. The multiple regression of the velocity gradient for the mentioned parameters.

Regression Statistics						
Multiple *R*	0.96					
R Square	0.91					
Adjusted *R* Square	0.87					
Standard Error	0.12					
Observations	33.00					
	df	*SS*	*MS*	*F*	Significance *F*	
Regression	11.00	3.32	0.30	20.08	0.00	
Residual	21.00	0.32	0.02			
Total	32.00	3.63				
	Coefficients	Standard Error	*t*-Stat	*P*-value	Lower *95%*	Upper *95%*
Intercept	4.83	0.37	12.97	0.00	4.05	5.60
ε	-3.17	0.61	-5.22	0.00	-4.44	-1.91
K^*	-0.07	0.10	-0.74	0.47	-0.28	0.13
M	0.02	0.01	1.23	0.23	-0.01	0.04
β	0.06	0.51	0.11	0.91	-1.00	1.12
λ	-0.04	0.15	-0.27	0.79	-0.35	0.27
S	0.08	0.02	3.77	0.00	0.04	0.13
Nb	-0.07	0.38	-0.20	0.85	-0.86	0.71
Nt	-0.07	0.38	-0.20	0.85	-0.86	0.71
A	-11.18	0.87	-12.90	0.00	-12.98	-9.37
J	-0.34	1.15	-0.29	0.77	-2.72	2.05
Ec	-0.08	0.29	-0.29	0.78	-0.68	0.51

The temperature gradient is positively correlated with the suction parameter and negatively correlated with ε, K^*, *Nb*, *Nt*, *A*, *J* and *Ec* but there is no correlation with *M* and β. The mass transfer rate is positively correlated with ε, *M*, β, *Nb*, *Nt*, and negatively correlated with λ, *S*, *J* and *Ec* but there is no correlation with K^* and *A*, respectively. It is also seen that the velocity gradient is positively correlated with the temperature gradient and negatively correlated with the concentration gradient. The temperature gradient is negatively correlated with the concentration gradient.

From Table 4 the multiple regression model for the velocity gradient can be written as

$$f''(0) = 4.83 - 3.17\varepsilon + 0.02M + 0.06\beta - 0.07K^* + 0.06\beta - 0.04\lambda + \\ -0.07Nb - 0.07Nt - 11.18A + 0.08S + 0.34J - 0.08Ec.$$

From Table 5, the multiple regression model for temperature gradient can be written as

$$\theta'(0) = 1.26 - 2.85\varepsilon - 0.01M + 0.12\beta + 0.04K^* - 0.6Q^* - 0.08Nb - 0.1Nt - 4.4A - \\ +3.88J - 0.04\lambda + 0.03S + 5.17Ec.$$

Table 5. The multiple regression of the temperature gradient for the mentioned parameters.

Regression Statistics						
Multiple *R*	*1.00*					
R Square	*0.99*					
Adjusted *R* Square	*0.99*					
Standard Error	*0.05*					
Observations	*33.00*					
	df	*SS*	*MS*	*F*	Significance *F*	
Regression	*11.00*	*6.07*	*0.55*	*216.09*	*0.00*	
Residual	*21.00*	*0.05*	*0.00*			
Total	*32.00*	*6.12*				
	Coefficients	Standard Error	*t*-Stat	*P*-value	Lower *95%*	Upper *95%*
Intercept	*1.26*	*0.15*	*8.23*	*0.00*	*0.94*	*1.58*
ε	*-2.85*	*0.25*	*-11.37*	*0.00*	*-3.37*	*-2.33*
K^*	*0.04*	*0.04*	*0.86*	*0.40*	*-0.05*	*0.12*
M	*-0.01*	*0.01*	*-1.10*	*0.28*	*-0.02*	*0.01*
β	*0.12*	*0.21*	*0.59*	*0.56*	*-0.31*	*0.56*
λ	*-0.04*	*0.06*	*-0.69*	*0.50*	*-0.17*	*0.09*
S	*0.03*	*0.01*	*3.80*	*0.00*	*0.02*	*0.05*
Nb	*-0.08*	*0.16*	*-0.49*	*0.63*	*-0.40*	*0.25*
Nt	*-0.10*	*0.16*	*-0.63*	*0.54*	*-0.42*	*0.23*
A	*-4.40*	*0.36*	*-12.33*	*0.00*	*-5.15*	*-3.66*
J	*-3.88*	*0.47*	*-8.22*	*0.00*	*-4.86*	*-2.90*
Ec	*5.17*	*0.12*	*43.76*	*0.00*	*4.92*	*5.41*

The multiple regression model for the concentration gradient can be written as

$$\varphi'(0) = -1.93 + 12.82\varepsilon + 0.26M + 6.68\beta - 0.95K^* + 4.8Nb + 35.73Nt - 0.77A - 25.09J + \\ -5.06Ec - 3.01\lambda - 0.99S.$$

Table 6. The multiple regression of the concentration gradient for the mentioned parameters.

Regression Statistics						
Multiple *R*	*0.67*					
R Square	*0.44*					
Adjusted *R* Square	*0.15*					
Standard Error	*3.56*					
Observations	*33.00*					
	df	*SS*	*MS*	*F*	Significance *F*	
Regression	*11.00*	*212.92*	*19.36*	*1.53*	*0.19*	
Residual	*21.00*	*265.83*	*12.66*			
Total	*32.00*	*478.75*				
	Coefficients	Standard Error	*t*-Stat	*P*-value	Lower *95%*	Upper *95%*
Intercept	*-1.93*	*10.81*	*-0.18*	*0.86*	*-24.41*	*20.55*
ε	*12.82*	*17.63*	*0.73*	*0.48*	*-23.85*	*49.48*
K^*	*-0.95*	*2.91*	*-0.33*	*0.75*	*-7.01*	*5.11*
M	*0.26*	*0.36*	*0.72*	*0.48*	*-0.49*	*1.01*
β	*6.68*	*14.77*	*0.45*	*0.66*	*-24.04*	*37.40*
λ	*-3.01*	*4.34*	*-0.69*	*0.49*	*-12.03*	*6.01*
S	*-0.99*	*0.64*	*-1.54*	*0.14*	*-2.31*	*0.34*
Nb	*4.80*	*10.95*	*0.44*	*0.67*	*-17.97*	*27.57*
Nt	*35.73*	*10.95*	*3.26*	*0.00*	*12.96*	*58.50*
A	*-0.77*	*25.16*	*-0.03*	*0.98*	*-53.08*	*51.55*
J	*-25.09*	*33.26*	*-0.75*	*0.46*	*-94.25*	*44.07*
Ec	*-5.06*	*8.31*	*-0.61*	*0.55*	*-22.35*	*12.23*

7. Conclusions

A boundary layer nanofluid slip flow over a stretching permeable wedge-shaped surface with viscous dissipation and Joule heating effect has been investigated numerically by using the SQLM with MATLAB software. From the simulations, the following conclusions can be drawn.

- The SQLM scheme by using the Chebyshev collocation method provides a more accurate and quicker convergence scheme.
- The momentum boundary layer thickness enhances with increasing values of the magnetic parameter, permeability parameter, and suction parameter but reduces for the Brownian motion, wedge angle parameter, and stretching ratio parameter.
- The thermal boundary layer thickness enhances with increasing values of the Brownian motion, thermophoresis parameter, Eckert number, Joule heating parameter, and heat generation parameter but squeezes for the suction parameter.
- The concentration boundary layer thickness enhances with increasing values of the thermophoresis parameter but shrinks with the Prandtl number, Lewis number, Brownian motion, heat generation parameter, and suction parameter.
- The skin friction coefficient increases by *4%*, *5%*, and *82%* due to increasing the magnetic parameter $(5.0-15.0)$ and suction parameter $(10.0-20.0)$ respectively. On the other hand, increasing the stretching ratio parameter $(0.0-0.4)$, wedge angle parameter $\left(36^\circ-72^\circ\right)$, and Brownian motion $(0.4-0.6)$ decreases the skin friction by *39.7%*, *5%* and *93.5%* respectively.

- For rising values of the stretching ratio parameter $(0.0-0.4)$ and suction parameter $(10.0-20.0)$, the heat transfer rate enhances by *3.5%* and *70%*, but for the Brownian motion $(0.4$ to $0.6)$, thermophoresis $(0.3-0.7)$ and wedge angle parameter $(0.3$ to $0.7)$ decrease the heat transfer rate by *133%*, *125%*, and *4%*, respectively.
- The skin friction coefficient is positively correlated with the magnetic parameter, permeability parameter, and suction parameter, but negatively correlated with the Brownian motion, wedge angle parameter, and stretching ratio parameter whereas there is no correlation with the mixed convection parameter, thermophoresis parameter, heat generation parameter, Prandtl number, and Eckert number.
- The temperature gradient is positively correlated with the magnetic parameter, permeability parameter, suction parameter, and stretching ratio parameter, but negatively correlated with the wedge angle parameter, Brownian motion, thermophoresis parameter, Eckert number, Joule heating parameter, and heat generation parameter, whereas there is no correlation with the mixed convection parameter.
- The concentration gradient is positively correlated with the Brownian motion, thermophoresis parameter, suction parameter, and Lewis number, but negatively correlated with the magnetic parameter and permeability parameter, whereas there is no correlation with the mixed convection parameter.

Nomenclature

A – velocity slip parameter

a – initial stretching constant

b – free stream constant

B_0 – strength of the magnetic field, A/m

BL – boundary layer

C – nanoparticle concentration, kg/m^3

C_f – skin friction coefficient

C_w – surface concentration, kg/m^3

C_∞ – free stream concentration

D_B – coefficient of Brownian motion, cm^2/s

D_B – coefficient of thermophoresis

J – Joule heating parameter

K – permeability, m^2

K^* – permeability parameter

g – acceleration due to gravity, m/s^2

Le – Lewis number

M – magnetic parameter

m – power-law index

MHD – magnetohydrodynamic

N – initial slip factor

Nb – Brownian motion

Nt – thermophoresis parameter

Nu_x – local Nusselt number

$ODEs$ – ordinary differential equations

$PDEs$ – partial differential equations

Pr – Prandtl number

Q^* – heat generation parameter

Sh_x – local Sherwood number

$SQLM$ – spectral quasi-linearization method

T – fluid temperature,

T_w – surface temperature,

T_∞ – free stream temperature

u – velocity component, m/s

U – free stream velocity

α – base fluid thermal diffusivity, m^2/s

β – wedge angle parameter

β^* – coefficient of thermal expansion

ε – stretching ratio parameter

v – fluid kinematics viscosity, m^2/s

v – y-axis velocity component, m/s ms-1

τ – ratio of the effective heat capacity

ρ – fluid density, kg/m^3

σ – electrical conductivity, s/m

ψ – stream function

Ω – total wedge angle

References

[1] Choi S.U.S. (1995): *Enhancing thermal conductivity of fluids with nanoparticles*.− Proc. ASME Int. Mech. Eng. Cong. Exp., San Francisco, USA, vol.66, pp.99-105.

[2] Buongiorno J. (2006): *Convective transport in nanofluids*.− ASME J. Heat Transfer, vol.128, pp.240-250.

[3] Falkner V.M. and Skan S.W. (1931): *Some approximate solutions of the boundary layer equations*.− Philosophical Magazine, vol.12, pp.865-896.

[4] Nagendramma V., Sreelakshmi K. and Sarojamma G. (2015): *MHD heat and mass transfer flow over a stretching wedge with convective boundary condition and thermophoresis*.− Proceedia Eng., vol.127, pp.963-96.

[5] Ashwini G. and Eswara A.T. (2015): *Unsteady MHD accelerating flow past a wedge with thermal radiation and internal heat generation/absorption*.− Int. J. Math. Com. Sci., vol.1, pp.13-26.

[6] Rames B.K.H., Shreenivas R.K., Achala L.N. and Bujurke N.M. (2017): *Similarity solutions of the MHD boundary layer flow past a constant wedge within porous media*.− Math. Prob. Eng., vol.2017, pp.11.

[7] Ibrahim W. and Tulu A. (2019): *Magnetohydrodynamic (MHD) boundary layer flow past a wedge with heat transfer and viscous effects of nanofluid embedded in porous media*.− Math. Prob. Eng., vol.2019, pp.12.

[8] Nageeb A., Haroun H., Mondal S. and Sibanda P. (2017): *Effects of thermal radiation on mixed convection in an MHD nanofluid flow over a stretching sheet using a spectral relaxation method*.− Int. J. Math. Com. Sci., vol.11, pp.1-10.

[9] Kasmani R.M., Sivasankaran S., Bhuvaneswari M. and Hussein A.K. (2017): *Analytical and numerical study on convection of nanofluid past a moving wedge with Soret and Dufour effects*.− Int. J. Num. Method Heat Fluid Flow, vol.27, pp.2333-2354.

[10] Waini I., Ishak A. and Pop I. (2020): *MHD flow and heat transfer of a hybrid nanofluid past a permeable stretching/shrinking wedge*.− Appl. Math. Mech., vol.41, pp.507 -520.

[11] Al-Sayagh R. (2021): *Control of the free convective heat transfer using a U-shaped obstacle in an Al_2O_3-water nanofluid filled cubic cavity*.− Int. J. Adv. Appl. Sci., vol.8, pp.23-30.

[12] Khan W.A. and Pop I. (2013): *Boundary layer flow past a wedge moving in a nanofluid*.− Math. Prob. Eng., vol.1, p.7, https://doi.org/10.1155/2013/637285.

[13] Menni Y., Chamkha A. J., Massarotti N., Ameur H., Kaid N. and Bensafi M. (2020): *Hydrodynamic and thermal analysis of water, ethylene glycol, and water-ethylene glycol as base fluids dispersed by aluminum oxide nano-sized solid particles*.− Int. J. Num. Methods Heat Fluid Flow, vol.30, pp.4349-4386.

[14] Krishna M.V., Ahamad N.A. and Chamkha A.J. (2021): *Hall and ion slip impacts on unsteady MHD convective rotating flow of heat generating/absorbing second-grade fluid*.− Alexandria Eng. J., vol.60, pp.845-885.

[15] Krishna M.V. and Chamkha A.J. (2020): *Hall and ion slip effects on unsteady MHD convective rotating flow of nanofluids - application in Biomedical Engineering*.− J. Egyptian Math. Soci., vol.28, pp.1-14.

[16] Krishna M.V., Ahamad N.A. and Chamkha A.J. (2020): *Hall and ion slip effects on unsteady MHD free convective rotating flow through a saturated porous medium over an exponentially accelerated plate*.− Alexandria Eng. J., vol.59, pp.565-577.

[17] Krishna M.V. and Chamkha A.J. (2020): *Hall and ion slip effects on MHD rotating flow of elastico-viscous fluid through a porous medium*.− Int. Commu. Heat Mass Transfer, vol.113, https://doi.org/10.1016/j.icheatmasstransfer.2020.104494.

[18] Krishna M.V. and Chamkha A.J. (2020): *Hall and ion slip effects on MHD rotating boundary layer flow of nanofluid past an infinite vertical plate embedded in a porous medium*.− Results in Physics, vol.15, p.10, https://doi.org/10.1016/j.rinp.2019.102652.

[19] Krishna M.V., Jyothi K. and Chamkha A.J. (2020): *Heat and mass transfer on MHD flow of second-grade fluid through porous medium over a semi-infinite vertical stretching sheet*.− J. Porous Media, vol.23, pp.751-765.

[20] Krishna M.V., Swarnalathamma B.V. and Chamkha A.J. (2019): *Investigations of Soret, Joule, and Hall effects on MHD rotating mixed convective flow past an infinite vertical porous plate*.− J. Ocean Engg. Sci., vol.4, pp.263-275.

[21] Krishna M.V., Reddy M.G. and Chamkha A.J. (2019): *Heat and mass transfer on MHD free convective flow over an infinite non-conducting vertical flat porous plate*.− Int. J. Fluid Mech. Res., vol.46, pp.1-25

[22] Krishna M.V., Swarnalathamma B.V. and Chamkha A.J. (2018): *Heat and mass transfer on the magnetohydrodynamic chemically reacting flow of micropolar fluid through a porous medium with Hall effects*.− Special Topics Rev. in Porous Media, Int. J., vol.9, pp.347-364.

[23] Krishna M.V., Anand P.V.S. and Chamkha A.J. (2019): *Heat and mass transfer on the free convective flow of a micropolar fluid through a porous surface with inclined magnetic field and Hall effects*.− Special Topics Rev. in Porous Media Int. J., vol.10, pp.203-223.

[24] Krishna M.V., Ahamad N.A. and Chamkha A.J. (2021): *Numerical investigation on unsteady MHD convective rotating flow past an infinite vertical moving porous surface*.− Ain Shams Eng. J., vol.12, pp.2099-2109.

[25] Motsa S.S., Dlamini P. and Khumalo M. (2014): *Spectral relaxation method and spectral quasilinearization method for solving unsteady boundary layer flow problems*.− Adv. Math. Phys., vol.2014, pp.1-12, https://doi.org/10.1155/2014/341964.

[26] Bellman R.E. and Kalaba R.E. (1965): *Quasilinearization and Nonlinear Boundary-Value Problems*.− Elsevier: New York, NY, USA.

[27] Mohammadi F., Hosseini M.M., Dehgahn A. and Ghaini F.M. (2012): *Numerical solutions of Falkner-skan equation with heat transfer studies*.− Nonlinear Sci., vol.3, pp.86-93.

Received: August 5, 2021
Revised: April 15, 2022